Published in final edited form as:
Nanomedicine (Lond). 2012 October ; 7(10): 1507–1519. doi:10.2217/nnm.12.27.

Antiangiogenic nanotherapy with lipase-labile *Sn-2* fumagillin prodrug

Dipanjan Pan*, **Nibedita Sanyal**, **Anne H Schmieder**, **Angana Senpan**, **Benjamin Kim**, **Xiaoxia Yang**, **Grace Hu**, **John S Allen**, **Richard W Gross**, **Samuel A Wickline**, and **Gregory M Lanza**
Division of Cardiology, Washington University School of Medicine, 4320 Forest Park Avenue, Saint Louis, MO 63108, USA

Abstract

Background—The chemical instability of antiangiogenic fumagillin, combined with its poor retention during intravascular transit, requires an innovative solution for clinical translation. We hypothesized that an *Sn-2* lipase-labile fumagillin prodrug in combination with a contact-facilitated drug delivery mechanism, could be used to address these problems.

Methods—$\alpha_v\beta_3$-targeted and nontargeted nanoparticles with and without fumagillin in the prodrug or native forms were evaluated *in vitro* and *in vivo* in the Matrigel™ (BD Biosciences, CA, USA) plug model of angiogenesis in mice.

Results—*In vitro* experiments demonstrated that the new fumagillin prodrug decreased viability at least as efficacious as the parent compound, on an equimolar basis. In the Matrigel mouse angiogenesis model, $\alpha_v\beta_3$-fumagillin prodrug decreased angiogenesis as measured by MRI (3T), while the neovasculature was unaffected with the control nanoparticles.

Conclusion—The present approach resolved the previously intractable problems of drug instability and premature release in transit to target sites.

Keywords

angiogenesis; fumagillin; nanomedicine; nanoparticle; prodrug; therapy

Fumagillin, a mycotoxin produced by *Aspergillus fumigatus*, has been demonstrated to suppress angiogenesis by inhibition of methionine aminopeptidase 2 (MetAP2) [1,2]. MetAP2 is one of two methionine aminopeptidase forms in eukaryotes, which are responsible for cleavage of the NH_2-terminal methionine residue from nascent proteins [3]. Although both MetAP1 and MetAP2 have common activity and substrates, only MetAP2 is upregulated during cellular proliferation [4]. MetAP2 has greater efficiency (1000-fold) catalyzing methionine removal from certain proteins, such as glyceraldehyde-3-phosphate, which can modulate subsequent activity, stability or subcellular localization [5,6]. TNP-470 is an acetylated, water-soluble, stable form of fumagillin that analogously alkylates His^{231} near the enzymatic center of MetAP2 to selectively inhibit proliferating endothelial cells (i.e., angiogenesis) and a subset of tumor cells, with little effect on nonendothelial cell types

*Author for correspondence: Tel.: +1 314 454 7674, Fax: +1 314 454 7490, dipanjan@wustl.edu.

Financial & competing interests disclosure
The authors have no other relevant affiliations or financial involvement with any organization or entity with a financial interest in or financial conflict with the subject matter or materials discussed in the manuscript apart from those disclosed.
No writing assistance was utilized in the production of this manuscript.

[2,7]. The anti-tumor efficacy of TNP-470 was demonstrated in a variety of rodent cancer models [8–11], but when tested in human clinical trials [12–15], the molecule possessed significant liabilities, including a brief systemic half-life for itself (2 min) and its primary metabolite AGM-1883 (6 min) [12] and moderately severe symptoms of neurotoxicity. Although fumagillin and its analogs are potent antiangiogenic compounds, significant reductions in dosage and new chemistry will be required to reduce adverse effects.

We have reported effective *in vivo* delivery of fumagillin with $\alpha_v\beta_3$-targeted perfluorocarbon (PFC) nanoparticles (NPs) at a fraction of the dosage required systemically for TNP-470 in previous preclinical and clinical studies [16–19]. In these studies, fumagillin was hydrophobically entrapped in the phospholipid surfactant, targeted to angiogenic endothelial cells, and delivered through a mechanism we described as contact-facilitated drug delivery (CFDD) [20]. Tethering of the NP to the target cell surface facilitated the interaction and hemifusion of the two lipid membranes, which facilitates the passive transfer of the drug and phospholipids from the NP surface to the outer leaflet of the target cell membrane. The drug is then translocated to the inner leaflet through an ATP-dependent mechanism [21,22]. CFDD eliminates the need for particle internalization with subsequent endosomal drug payload escape or extracellular particle release with diffusion into the cell. $\alpha_v\beta_3$-targeted fumagillin PFC NPs have been shown to prolong the pharmacodynamic antiangiogenic effect in preclinical models of atherosclerosis and arthritis [19,23–25]. It is noteworthy that this nanomedicine approach to antiangiogenesis has both high potency and prolonged effectiveness, even when compared with the newest analogs of fumagillin, for example, PPI-2458, which were administered daily for effectiveness in arthritis [26].

Despite these promising *in vivo* results, the ‘drugability’ of native fumagillin is compromised by chemical instability associated with two highly reactive epoxide rings at the active site and a photosensitive conjugated decatetraenedioic tail. The fumagillin chromophore is reported to be photolytically and stoichiometrically transformed by first-order rates to new chromophoric analogs (‘neofumagillin[s]’) for which the apparent absorptivities are diminished and maxima are shifted into the violet region [27]. Moreover, parallel pharmacokinetic tracking of $\alpha_v\beta_3$-targeted fumagillin PFC NP components revealed substantial premature loss of the drug during circulation to the target despite its low aqueous solubility and high *in vitro* retention during dissolution studies (Supplementary figure 1; see online www.futuremedicine.com/doi/suppl/10.2217/nnm.12.27).

The objective of this study was to develop a nanomedicine centric approach to address fumagillin photoinstability, to prevent premature intravascular drug release in circulation, and to achieve effective intracellular transport through CFDD when bound to the target cell using an *Sn-2* lipase-labile phospholipid prodrug (PD). We hypothesized this novel fumagillin analog would provide a stable membrane complex within the NP phospholipid membrane during circulatory transit to the target sites and upon binding to the target endothelial cells, transfer to the cell membrane by CFDD and the formation of hemifusion complex. Within the cell membrane, the PD would be susceptible to intracellular phospholipase liberation. Moreover, from a pharmaceutical translation perspective, we hypothesize a facile synthesis (Figure 1) for the fumagillin-PD (Fum-PD) that would eliminate the light-mediated photodegradation attributed to the conjugated decatetraenedioic tail group.

Materials & methods

Materials

Unless otherwise listed, all solvents and reagents were purchased from Aldrich Chemical Co. (MO, USA) and used as received. Anhydrous chloroform was purchased from Aldrich

Chemical Co. and distilled over calcium hydride prior to use. Biotinylated dipalmitoyl-phosphatidylethanolamine and high purity egg yolk phosphatidylcholine were purchased from Avanti Polar Lipids, Inc. (AL, USA). Perfluorooctylbromide was purchased and used as received from Exfluor Research Corporation (TX, USA). Fumagillin was obtained as a dicyclohexylamine salt from NCI as a gift [201]. Argon and nitrogen (UHP; 99.99%) were used for storage of materials. The Spectra/Por membrane (Cellulose MWCO: 20,000 Da) used for dialysis was obtained from Spectrum Medical Industries, Inc. (CA, USA).

Preparation of *Sn-2* phospholipase-labile Fum-PD

Synthesis of the *Sn-2* PD was accomplished in two steps:

- Saponifying fumagillin dicyclohexylamine salt to fumagillol;
- Esterifying the product with 1-palmitoyl-2-azelaoyl-sn-glycero-3-phosphocholine.

Fumagillin dicyclohexylamine salt was suspended in 1:1 methanol:water and treated with 35% NaOH solution (Figure 1). The dark-brown mixture was stirred in an ice bath for 2 h, warmed to room temperature and then treated with another equivalent of NaOH solution. The mixture was stirred until starting material was not detected by thin layer chromatography (~4 h); the methanol was evaporated and the residue extracted into ethyl acetate. The mixture was then extracted with 5% citric acid, brine, bicarbonate and brine again, then dried with $MgSO_4$ and concentrated *in vacuo*. The crude product was further purified with activated charcoal in acetonitrile then filtered through a celite pad (yield: a colorless solid, 59 mg [70%]). ^{1}H NMR (CD_3OD): δ 5.20 (t, 1H), 4.3 (m, 1H), 3.42 (m, 1H), 3.38 (s, 3H), 2.88 (d, 1H), 2.63 (t, 1H), 2.51 (d, 1H), 2.1–2.3 (m, 2H), 2.2 (m, 1H), 1.89 (d, 1H), 1.7–1.9 (m, 2H), 1.8 (d, 3H), 1.7 (d, 3H), 1.17 (s, 3H), 0.96 (m, 1H). HR-MS found: MH+ (283.3).

A solution of C16–09:0 (COOH) phosphatidylcholine 1-hexadecyl-2-azelaoyl-sn-glycero-3-phosphocholine followed by DMAP and DCC was added to a solution of fumagillol in dry dichloromethane. The reaction mixture was stirred overnight at ambient temperature then passed over a short pad of silica gel using EtOAc/n-hexane. The filtered solvent was removed *in vacuo*, leaving an oil residue that was purified by column chromatography on SiO_2 with EtOAc/n-hexane as the elution solvent to give the Fum-PD 1 compound as a pale yellowish solid (yield: 54%). ^{1}H NMR ($CDCl_3$): δ 0.88 (t, 3H), 1.22–1.37 (m, 37H), 1.58–1.96 (m, 20H), 2.26–2.60 (m, 7H), 3.40 (m, 12H), 3.48 (m, 3H), 3.86–4.00 (m, 4H), 4.10–4.37 (m, 5H), 5.21 (m, 1H). HR-MS found: 930.6 (MH+).

To assess photostability, the PD was dissolved in anhydrous ethanol, irradiated with UV for 2 h and the degradation products were determined by electrospray ionization mass spectrometry, which confirmed that the drug completely retained its chemical integrity.

Preparation of $\alpha_v\beta_3$-targeted fumagillin NPs

PFC NPs were prepared as a microfluidized suspension of 20% (v/v) 15:5 perfluorocrown ether (Exfluor Inc., TX, USA), 2.0% (w/v) of a surfactant comixture and 1.7% (w/v) glycerin in pH 6.5 carbonate buffer. An $\alpha_v\beta_3$-integrin antagonist, a quinalone nonpeptide developed by Bristol-Myers Squibb Medical Imaging (US patent US6511648 and related patents) [101], was used for homing angiogenesis. The surfactant comixture of NPs included: approximately 97.6 mole% lecithin, 0.15 mole% of $\alpha_v\beta_3$-ligand-conjugated lipid and 2.28 mole% of Fum-PD (~0.5 μM). For MRI, the surfactant excluded the Fum-PD but included 20 mole% gadolinium-DOTA-phosphoethanolamine. Nontargeted NPs excluded the homing ligands. The surfactant components for each formulation were combined with the PFC, buffer and glycerin with pH adjusted to 6.5, and the mixtures were homogenized at

20,000 psi for 4 min. The NPs were preserved under inert gas in sterile sealed vials until use. For *in vitro* and *in vivo* evaluation, four NP formulations were prepared: $\alpha_v\beta_3$-targeted Fum-PD PFC NPs ($\alpha_v\beta_3$-Fum-PD-NP), $\alpha_v\beta_3$-targeted fumagillin PFC NPs ($\alpha_v\beta_3$-Fum-NP), $\alpha_v\beta_3$-targeted no drug PFC NPs ($\alpha_v\beta_3$-ND-NP), or nontargeted Fum-PD PFC NPs (NT-Fum-PD NP).

The $\alpha_v\beta_3$-integrin antagonist was initially reported as the ^{111}In-DOTA conjugate RP748 and cyan 5.5 homologue TA145. The $\alpha_v\beta_3$ ligand has a 15-fold preference for the Mn^{2+} activated receptor (21 nmol/l) and the IC_{50} of the NP for inhibition of β3 integrin expressing cell binding to vitronectin was 50 pM [Kereos Inc., MO, USA, Data on File]. The increased affinity of the NPs is attributed to the high copy number of peptidomimetics on the particle, which allows for multivalent binding.

Characterization of $\alpha_v\beta_3$-targeted fumagillin NP

Dynamic light scattering measurements revealed that the nominal hydrodynamic diameters (D_h) of the $\alpha_v\beta_3$-targeted Fum-PD PFC NP and control samples in aqueous solution were within 220–280 nm. Incorporation of PD at 2.28 mole% (~0.5 μM) within the surfactant comixture resulted in negligible changes in particle sizes (Figure 1). Zeta potential values (Brookhaven Instrument Co., NY, USA) of the NPs were negative (ca. −25 mV), which confirms successful phospholipid encapsulation.

These NPs exhibit excellent shelf-life stability with very negligible changes noticed in particle diameter after a long shelf life (typically 6 months). *In vitro* dissolution revealed the PD was well retained with only <10% of the incorporated dosage diffusing from the NP under infinite sink conditions during *in vitro* dissolution. The majority of drug release occurred during the first day (4.5%) with further losses undetectable between days 2 and 7.

In vitro HUVEC studies to confirm Fum-PD bioavailability & bioactivity

Human umbilical vein endothelial cells (HUVECs; Lonza, MD, USA), between passages 2 to 6, were seeded on a 96-well plate (5000 cells/well). After 24 h, cells were incubated with $\alpha_v\beta_3$-Fum-PD-NP, $\alpha_v\beta_3$-targeted native fumagillin PFC NP ($\alpha_v\beta_3$-Fum-NP), $\alpha_v\beta_3$-ND-NP, or NT-Fum-PD-NP for 1 h (six replicates per sample per plate). Wells were washed three-times with phosphate-buffered saline (PBS), and plates were returned to the incubator. From 2 to 4 days after drug exposure, the following assays were used to test the effect on cell metbolism and proliferation.

Cell proliferation was measured using CyQuant NF cell proliferation kit (Invitrogen; CA, USA), which measures cellular DNA content via fluorescent dye binding. Cell metabolic activity was measured using an Alamar Blue (Invitrogen), which is based on the reduction of nonfluorescent dye to fluorescent substrate in metabolically active cells. This reduction is typically attributed to different oxidoreductase enzyme systems that use NAD(P)H as the primary electron donor. The redox reaction was monitored using a fluorescence plate reader (excitation 570 nm and emission 587 nm) where the resulting signal is proportional to the number of viable cells present. Signal intensity from each sample was normalized to the control ($\alpha_v\beta_3$-ND-NP; n = 3–6 plates per time point).

In vivo Matrigel™ implant model of angiogenesis in *Rag1^{tm1Mom}* Tg(TIE-2-lacZ)182-Sato mice

All animal studies were conducted in accordance with a protocol approved by the Washington University of Saint Louis Animal Studies Committee. Matrigel was implanted into a cohort of *Rag1^{tm1Mom}* Tg(TIE-2-lacZ)182-Sato mice (Jackson Labs, ME, USA) to confirm localization of $\alpha_v\beta_3$-targeted native PFC NP ($\alpha_v\beta_3$-ND-NP) to nascent angiogenic

endothelium (Tie-2^-; platelet endothelial cell adhesion molecule [PECAM]$^+$) versus stabilized maturing microvessels (Tie-2^+; PECAM$^+$) [28]. Mice were anesthetized with a mixture of ketamine (85 mg/kg) and xylazine (15 mg/kg), maintained on 0.75–1.0% isoflurane, and injected with 1 ml of Matrigel containing 500 ng FGF (± 100 ng MCP-1) and 64 U heparin. On day 16, the mice were reanesthetized and administered rhodamine-labeled $\alpha_v\beta_3$-ND-NP via tail vein injection. After 2 h the animals were euthanized. The Matrigel plugs were excised and frozen in OCT for cryosectioning.

Frozen sections (10 μm) were studied with an Olympus BX61 microscope and a F-View II camera using a Cy3.3 filter. The cell nuclei were counterstained with DAPI. Immunohistochemistry for endothelial PECAM-1 (CD31) was performed on adjacent frozen sections (clone MEC13.3, BD Biosciences, CA, USA) developed with ABC method and VIP substrate kits (Vector Laboratories, CA, USA) and counterstained with Methyl Green. Hematoxylin and eosin staining was performed using routine histochemistry methods.

For Lac-Z staining of the Tie-2 receptor, 10-μm sections were fixed in 2% paraformaldehyde, 0.125% glutaraldehyde in PBS for 5 min. Fixative was aspirated and the slides were incubated three-times for 1 min each in 2 mM $MgCl_2$ in PBS. Slides were incubated three-times for 2 min in a PBS mixture (50 ml) containing $MgCl_2$ (2 mM), 0.02% nonyl phenoxypolyethoxylethanol (10 μl; NP40) and desoxycholate (5 mg). Subsequently, the slides were placed in staining buffer [202] without 5-bromo-4-chloro-3-indolyl-beta-D-galactopyranoside (X-gal) for 2 min followed by the addition of X-gal overnight at 37°C. Light images were captured with a ColorView II camera.

In vivo MR evaluation using the Matrigel implant model of angiogenesis in rats

Angiogenesis was evaluated using a Matrigel plug model in Sprague–Dawley rats. Adult Sprague–Dawley rats (250–350 g) were anesthetized with a mixture of ketamine (85 mg/kg) and xylazine (15 mg/kg) and maintained on 0.75–1.0% isoflurane delivered through a calibrated vaporizer. Anesthetized flank-shaven rats were injected with 1 ml of Matrigel containing 500 ng FGF (± 100 ng MCP-1) and 64 U heparin. On days 9, 11 and 13 postimplant rats were treated (2 ml/kg intravenous) with $\alpha_v\beta_3$-Fum-PD-NP (~0.5 μM), $\alpha_v\beta_3$-Fum-NP (~0.5 μM), $\alpha_v\beta_3$-ND-NP (0.0 μM), or NT-Fum-PD NP (~0.5 μM). On day 15, angiogenesis was assessed in anesthetized animals (as above) by MR molecular imaging at 3T (Philips Achieva; Amsterdam, The Netherlands) with $\alpha_v\beta_3$-integrin paramagnetic NPs. A SENSE-FlexM coil using a high-resolution, T_1-weighted, fat-suppressed, 3D gradient echo sequence. Images were obtained before and 20, 60 and 90 min after intravenous administration of $\alpha_v\beta_3$-paramagnetic NPs (1 ml/kg) to compare the antiangiogenic influence of the four treatments.

Image processing—In each experiment, the signal intensities of the MR images were analyzed with custom MATLAB software (The Math Works, MA, USA). Dynamic T_1-weighted signal intensities were normalized to a Gd-DTPA doped water reference standard included within each imaging field of view. For each animal, a region of interest was manually placed around the Matrigel implant on each baseline slice, and the signal intensity means and standard deviation were calculated. Subsequently, serial images were spatially co-registered using a cross-correlation routine, and the tumor region of interest mask was copied to each time point. Voxels at 90 min with an MR signal intensity increase at least three standard deviation above the baseline implant signal were considered enhanced. The percentage of implant volume enhanced was determined for each animal, averaged for each group, and compared across treatments.

Histology—Following MRI, the Matrigel implants were excised and processed as above to assess the overall microvessel density between the $\alpha_v\beta_3$-Fum-PD-NP (treated) and $\alpha_v\beta_3$-ND-NP (control). Briefly, frozen sections (10 μm) were studied with an Olympus BX61 microscope and a F-View II camera using a Cy3.3 filter. Immunohistochemistry for endothelial PECAM-1 and anti-alpha smooth muscle actin (Sigma, clone 1A4; α-SMA) was performed on adjacent frozen sections developed with ABC method and VIP substrate kits. Hematoxylin and eosin staining was performed using routine histochemistry methods.

Statistical analysis

Data were analyzed using general linear models procedures (SAS Inc., NC, USA) with means separations performed using Tukey–Kramer and Dunnett's ($p < 0.05$) techniques. Data are presented as the mean ± standard error of the mean unless otherwise stated.

Results

In vitro HUVEC studies to confirm Fum-PD bioavailability & bioactivity

The effectiveness of $\alpha_v\beta_3$-targeted Fum-PD PFC NPs was determined *in vitro* using cell proliferation and cell metabolic activity measurement assays. HUVECs were incubated for 60 min with $\alpha_v\beta_3$-Fum-PD-NP, $\alpha_v\beta_3$-Fum-NP, $\alpha_v\beta_3$-ND-NP, or NT-Fum-PD NP. Cell proliferation at 48, 96 and 120 h was reduced at 48 h equivalently for the integrin-targeted PFC NPs incorporating either the native or Fum-PD, revealing that the *Sn-2* lipase-labile phospholipid PD was equally bioavailable and effective to the native compound *in vitro* (Figure 2B). At 72 h, the effectiveness of the $\alpha_v\beta_3$-Fum-PD-NP and $\alpha_v\beta_3$-Fum-NP treatments relative to the control ($\alpha_v\beta_3$-ND-NP) persisted, and a numerically less but significant decrease in cell proliferation was appreciated in the NT-Fum-PD NP wells. This response was not unexpected *in vitro*, since the PFC NPs have a density of 1.98 g/ml, twice that of water, and have a tendency to settle and entrap along exposed edges, despite careful repeated washing. Intimate contact between the drug-rich and the cell membrane can CFDD, hemifusion, lipid transfer and drug delivery, albeit less effectively than with ligand-based binding. No reduction of cell density below the initial seeding was appreciated in any group (data not shown). HUVEC metabolic activity at 48, 96 and 120 h also revealed that the $\alpha_v\beta_3$-Fum-PD-NP was effective at each timepoint (Figure 2A). At 48 h, both $\alpha_v\beta_3$-Fum-PD-NP and $\alpha_v\beta_3$-Fum-NP reduced ($p < 0.05$) the activity of HUVEC cells versus the control or NT-Fum-PD NP groups. Although at 96 h only the $\alpha_v\beta_3$-Fum-PD-NP decreased metabolic activity versus control, at 120 h $\alpha_v\beta_3$-Fum-PD-NP and $\alpha_v\beta_3$-Fum-NP both decreased ($p < 0.05$) metabolic activity. Again the $\alpha_v\beta_3$-targeted *Sn-2* phospholipase-labile PD NPs had equivalent effectiveness *in vitro* compared with the $\alpha_v\beta_3$-targeted native fumagillin NPs as used in several previous studies [16,18,19,23–25]. Collectively, these data affirm the sensitivity of proliferating endothelial cells to the effects of fumagillin, either in the native or PD form.

In vivo Matrigel implant model of angiogenesis in *Rag1*^{tm1Mom} Tg(TIE-2-lacZ)182-Sato mice

Microscopic characterization of the $\alpha_v\beta_3$-PFC NPs in the Matrigel model was pursued using a separate cohort of *Rag1*^{tm1Mom} Tg(TIE-2-lacZ)182-Sato mice. Matrigel plug angiogenesis was targeted with rhodamine-labeled $\alpha_v\beta_3$-PFC NPs *in vivo* then the plug was excised for fluorescent and light microscopy visualization 2 h later (Figure 3). Figure 3A presents a low power hematoxylin and eosin stained example of an excised Matrigel plug. Fluorescent microscopy revealed the marked accumulation of rhodamine $\alpha_v\beta_3$-PFC within the plug (Figure 3D). PECAM staining demonstrated abundant microvascularity in this region (Figure 3B). In Figure 3C, Lac-Z staining, which was regulated by the Tie-2 promoter, was negligible, seen in only one vessel along the periphery distinct from regions with prevalent

rhodamine $\alpha_v\beta_3$-PFC. These data indicate that the $\alpha_v\beta_3$-PFC NPs are specific for ($PECAM^+$, $Tie\text{-}2^-$) angiogenic endothelium induced by the Matrigel growth factors and not for more mature microvessels ($PECAM^+$, $Tie\text{-}2^+$) seen in muscle and peripheral tissues (not shown).

In vivo MR evaluation using a Matrigel implant model of angiogenesis in rats

Next, using an *in vivo* Matrigel plug model in rats, we demonstrated the concept of antiangiogenesis treatment with $\alpha_v\beta_3$-targeted Fum-PD NPs and quantified therapeutic response using MRI neovascular mapping at 3T with $\alpha_v\beta_3$-targeted paramagnetic PFC NPs, as previously reported [16,18,19,23–25]. Following serial treatment on days 9, 11 and 13 days postimplant with $\alpha_v\beta_3$-Fum-PD-NP (~0.5 μM), $\alpha_v\beta_3$-Fum-NP (~0.5 μM), $\alpha_v\beta_3$-ND-NP (0.5 μM), or NT-Fum-PD NP (~0.5 μM), angiogenesis was assessed on day 15. Marked signal enhancement of angiogenic vasculature was evident and equivalent ($p > 0.05$) in animals receiving $\alpha_v\beta_3$-Fum-NP, $\alpha_v\beta_3$-ND-NP, or NT-Fum-PD-NP, but very little ($p < 0.05$) contrast was appreciated in rats given the integrin-targeted Fum-PD ($\alpha_v\beta_3$-Fum-PD-NP) (Figure 4A–D). Angiogenesis was detected by MR 30 min after injection of $\alpha_v\beta_3$-Fum-NP, $\alpha_v\beta_3$-ND-NP, or NT-Fum-PD NP and persisted through the remainder of the dynamic imaging period (60 min) without significant change (Figure 4E). In contradistinction, contrast in animals injected with $\alpha_v\beta_3$-Fum-PD-NPs was very low, compared with the other treatments throughout the imaging interval. This low level of signal likely reflects the recrudescence of neovessels between day 13, the last PD treatment, and day 15.

Microscopic examination of the excised Matrigel plugs from the $\alpha_v\beta_3$-Fum-PD-NPs (treated) and $\alpha_v\beta_3$-ND-NPs (control) showed a visually apparent difference in the peripheral plug density of α-SMA/$PECAM^+$ vessels in the control versus the treated animals (Figure 5). These data suggest that serial treatment with the Fum-PD continually suppressed the maturation of neovessels around the Matrigel plug, whereas in the control both new neovessels (i.e., assessed by MRI) and a maturing microvessel network (α-SMA-positive vessels) progressively developed.

Discussion

The development of ligand-directed therapeutic nanomedicines, theranostic or otherwise, entails several implicit goals that define the purity, potency and proper dosage of the drug delivery system at the target site. First, the active pharmaceutical ingredient (API) must be incorporated stably into the particle in a defined chemical form, within the intended 3D spatial location, and at the appropriate concentration. This NP formulation, under optimized storage conditions, must remain essentially unchanged for months to years, resisting spontaneous hydrolysis, Ostwald ripening, aggregation, or fusion of particle dependent on the chemistry; similarly, losses of the API whether due to early release into the excipient or chemical changes must be controlled. When administered *in vivo*, regardless of route, the particle and its payload must remain essentially intact during transit to the target cell, recognizing that much of the agent will be lost during the distribution phase through natural clearance mechanisms, such as phagocytosis by the reticuloendothelial system. Unfortunately, the common marked premature release of drug within the first few minutes of injection undermines safety and efficacy benefits of targeted agents. However, it must be recognized that many nontargeted agents serve primarily as excipients or as a means to constrain drug biodistribution and alter pharmacokinetics. Finally, upon reaching the target cell, the drug must be effectively transferred from the particle to the cell cytosol with high efficiency, bioavailability and bioactivity.

As discussed previously, fumagillin, a very hydrophobic compound, has been dissolved into the phospholipid surfactant of PFC NPs and used effectively for antiangiogenesis therapy in

multiple preclinical cancer, atherosclerosis and arthritis studies [16,18,19,23–25]. Although the chemical fragility of fumagillin is well known, laboratory handling techniques were adopted to guard against hydrolysis or photodegradation during handling, synthesis and storage of the active compound and the NP. However, further *in vivo* pharmacokinetics studies revealed a rapid blood loss of the dissolved API relative to the other nanoparticle components. Although academically the principles of theranostic nanomedicine could be pursued, pharmaceutical development and clinical translation of this concept was compromised, which inspired the *de novo* design and development of the *Sn-2* phospholipase-labile Fum-PDs in combination with CFDD using the integrin-targeted PFC NP.

As noted in Figure 1, the synthesis of fumagillin into the PD involved saponifying fumagillin to fumagilol, which preserved the critical di-epoxide active moiety of the molecule while eliminating the photosensitive conjugated decatetraenedioic tail group. Under this condition, the epoxy groups were found to be structurally intact, which was also similarly evidenced by other groups [29]. This tail group was effectively substituted by the seven-carbon *Sn-2* acyl groups of the phosphatidylcholine backbone, that is, 1-palmitoyl-2-azelaoyl-sn-glycero-3-phosphocholine. As shown, the synthesis of the PD followed an elegant two-step, one-pot procedure that is easily scalable to clinical production levels. Moreover, the removal of fumagillin's photosensitivity created a pharmaceutically relevant API with acceptable storage and handling properties. As a phospholipid compound, the self assembly of the PD into lipid surfactant of the PFC NP, or any similar lipid particle, was easily accomplished. The resultant particle was very stable, and essentially unchanged physicochemically from the drug-free particles at API inclusion levels up to 2 mole% of the surfactant. Given the potency of the API, higher concentrations have never been required, and often, much lower payloads were equally effective [16,18,19,23–25].

The retention of the Fum-PD in the particle during *in vitro* dissolution was excellent, very similar to the results obtained with the native fumagillin (Supplementary figure 1). In related pilot studies (data not shown), *Sn-2* phospholipase PDs incorporated into PFC NPs were stable in serum alone or enriched with exogeneous phospholipase A2. Lipase liberation of the drug *in vitro* required the addition of isopropyl alcohol to 'crack' the emulsion in order to expose the surfactant components to the enzyme. Thus, in $\alpha_v\beta_3$-Fum-PD-NP the API is nestled into the hydrophobic phospholipid layer and protected from hydrolysis and lipase activation in transit to the target.

Upon reaching the target cell, binding of the particle to surface receptor brings the drug-rich surfactant and cell membrane into close proximity (i.e., CFDD), which favors hemifusion and translation of the surfactant components into the outer membrane leaflet. Phospholipids from PFC NP transfer into the inner cell membranes, in an ATP-dependent process, and distribute throughout the interconnected internal membrane architecture. Interestingly, phospholipids (e.g., phosphatidylethanolamine) modified to present molecules on the particle surface, such as phospholipid-anchored gadolinium chelates, transfer to the outer target cell membrane passively but were not 'flipped' into the inner membrane leaflet and distribute throughout the cytosolic membranes. Instead, the metal chelates were found rapidly cleared from the body through the kidneys [Kereos Inc., MO, USA, Data on File]. For a similar reason, drugs attached to the surface of the NPs have retained excellent stability in circulatory transit, like the gadolinium chelates, but bioavailability at the target was very poor, even when highly enzymatic labile groups were inserted to encourage local drug release [Kereos Inc., MO, USA, Data on File].

Once the *Sn-2* Fum-PD has entered the cell, the liberation by enzymes resulted in equivalent bioavailability of native API and the PD API, perhaps numerically favoring the PD (Figure

2). Using the Matrigel plug model of angiogenesis, the effectiveness of the integrin-targeted Fum-PD ($\alpha_v\beta_3$-Fum-PD-NP) was clearly demonstrated to be superior to the nontargeted PD (NT-Fum-PD NP), targeted fumagillin ($\alpha_v\beta_3$-Fum-NP) and control ($\alpha_v\beta_3$-ND-NP) NP based on MR angiogenesis molecular imaging. The very poor effectiveness of the $\alpha_v\beta_3$-Fum-NP was related to the more rapid clearance of the PFC NPs in rodents than rabbits [30] and the anticipated premature loss of the API. These data emphasized the benefits of the $\alpha_v\beta_3$-Fum-PD-NP formulation *in vivo*, which experienced the same pharmacokinetics but retained and delivered the PD payload at efficacious dosages to the target cells (Figure 4). Microscopic examination of the excised Matrigel following MRI acquisition revealed prominent α-smooth muscle actin staining of the maturing microvessels along the periphery of the implant in the controls, which was notably diminished in the targeted PD-treated rats. This observation likely reflects the repeated pruning of neovessels in the treated animals through serial dosing, while microvascular development was essentially unimpaired in the controls.

The enzyme(s), mechanisms and rate controlling elements affording the release of the fumagillin into the cytosol from the membrane have still to be elucidated. Phospholipases A2 (PLA_2) is a superfamily of enzymes that catalyze the hydrolysis of the *Sn-2* ester bond in a variety of phospholipids releasing a free fatty acid and a lysophospholipid. These enzymes are classified as five major types: secreted low molecular weight sPLA_2s, larger cytosolic Ca^{2+}-dependent cPLA_2s, Ca^{2+}-independent iPLA_2s, platelet-activating factor acetylhydrolases and lysosomal PLA_2s [31]. The hydrolysis of the *Sn-2* ester bond represents the first step in the pathway to many second messengers, for example, the conversion of liberated arachadonic acid into eicosanoids, which exert a wide range of physiological and pathological effects. In endothelial cells, multiple family members of most of the different types of phospholipases are present thereby creating a rich repertoire of potential activating agents within target cells. Moreover, in addition to these known types of lipases in endothelial cells, additional serine hydrolases (or other hydrolases) are present, which could liberate the PD to active drug in target cells.

Although the concept of *Sn-2* phospholipid PDs has never been considered for targeted drug delivery as presented here, a precedence for the formation of *Sn-2* phospholipids PDs was found for two compounds, indomethacin and valproic acid [32,33]. In these studies, *Sn-2* phospholipid conjugates were utilized to effect oral controlled release of drugs by continuous degradation of the phospholipids PD within the intestine. Unfortunately, oral administration of an indomethacin PD decreased the total amount of drug absorbed in comparison to the administration of free indomethacin, although it smoothed the plasma concentration versus time profile curve, delaying T_{max} and lowering C_{max} [33]. When the PD was administered intravenously as an untargeted liposome, the bioavailability of the PD was further reduced relative to oral administration of the phospholipid PD and free drug. Direct attachment of indomethacin to the *Sn-2* ester completely blocked PLA_2 hydrolysis activity, while inserting short spacers between the drug and the ester bond greatly improved activity. The longest spacer assessed was five carbons. Analogous results were obtained for valproic acid PD studied similarly [32].

In follow-on research to this work, Jorgensen pursued the use of untargeted liposomes containing a *Sn-2* PDs, anticipating that increased secretory phospholipase liberated by cancers would facilitate the release of the API in the proximity of a tumor increasing the local drug concentration [34–38]. The effectiveness of this approach was modest and further enhancement by utilizing thermosensitive untargeted PD liposome with exogeneous heating was limited [34]. These investigators noted that the native liposome, which is highly susceptible to intravascular clearance and destruction, was more resistant to PLA_2 drug liberation, than the commonly used stealth or pegylated liposomes, suggesting that the PEG

facilitated the affinity of PLA_2 to the particles. Thus, the pegylation of liposomes required to extend intravascular circulation undesirably predisposes the vesicles to premature drug release by PLA_2. In general, the efficacy of the liposomal *Sn-2* PDs liberation by secretory phospholipases was dependent on water accessibility to the bond, which was less for the synthetic ether-lipid PDs studied than natural lipids. For the targeted PFC NPs, the reduced water accessibility of the *Sn-2* Fum-PD is highly desirable, preventing premature release or metabolism until the ligand-directed CFDD mechanism of drug delivery ensues.

Conclusion

Although we have repeatedly demonstrated the efficacy of fumagillin incorporated into the lipid surfactant of integrin-targeted perfluorochemical NPs in a variety of preclinical models, the photochemical instability [27,39] of the compound combined with its low retention during intravascular transit to the target required the innovation of an *Sn-2* lipase-labile PD solution. The synthesis of the *Sn-2* PD was accomplished in two steps, which produced a photochemically stable form of fumagillin that was easily and stably incorporated into the phospholipid surfactant of PFC NPs. $\alpha_v\beta_3$-targeted Fum-PD NP had high bioavailability and efficacy, equivalent to the native drug *in vitro* against proliferating HUVEC, and superior to the same in the Matrigel plug model of angiogenesis. Microscopic studies characterized and corroborated the specificity of the $\alpha_v\beta_3$-targeted NP for nascent neoendothelium (i.e., Tie-2 negative, $PECAM^+$) for drug delivery and molecular imaging. Further examination of the Matrigel plug following serial treatment with the therapeutic NPs and MRI of angiogenesis corroborated the repeated neovessel pruning effect of the targeted Fum-PD in comparison with the extensive maturing microvasculature appreciated around the Matrigel implant periphery in the control animals. Although the concept of incorporating a drug molecule into phospholipids has been previously reported by others, for example, Szoka and coworkers [40]; for fumagillin, and likely for many other drugs, the *Sn-2* PD approach combined with CFDD resolved a previously intractable problem of NP drug retention in the vasculature combined with high efficiency intracellular drug delivery at the targeted site. This new approach is highly conducive to pharmaceutical translation of nanomedicine-based antiangiogenesis therapy into the clinic.

Future perspective

Molecular imaging of angiogenesis with integrin-targeted PFC NPs is currently ongoing in US Phase I clinical studies. Following success at this level, the follow-on introduction of the antiangiogenesis therapy product is anticipated. While the API of this formulation is not resolved, the *Sn-2* PD approach is highly amenable to controlled scale-up and clinical translation. The combination of the two products could provide validated imaging and therapy nanomedicine technologies applicable to cancer, atherosclerosis and arthritis.

Supplementary Material

Refer to Web version on PubMed Central for supplementary material.

Acknowledgments

This research was supported by grants from the AHA (0835426N and 11IRG5690011) and NIH (NS059302, CA119342, CA1547371, NS073457, HL073646, HL078631 and N01CO37007).

References

Papers of special note have been highlighted as:

■ of interest

■■ of considerable interest

1. Sin N, Meng L, Wang MQ, Wen JJ, Bornmann WG, Crews CM. The anti-angiogenic agent fumagillin covalently binds and inhibits the methionine aminopeptidase, MetAP-2. Proc. Natl Acad. Sci. USA. 1997; 94(12):6099–6103. [PubMed: 9177176] ■■ Introduces the antiangiogenic effect of fumagillin and mechanistic insight into MetAP-2-binding.
2. Liu S, Widom J, Kemp CW, Crews CM, Clardy J. Structure of human methionine aminopeptidase-2 complexed with fumagillin. Science. 1998; 282(5392):1324–1327. [PubMed: 9812898] ■ Structural elucidation of fumagillin complexation with human MetAP-2.
3. Arfin SM, Kendall RL, Hall L. Eukaryotic methionyl aminopeptidases: two classes of cobalt-dependent enzymes. Proc. Natl Acad. Sci. USA. 1995; 92(17):7714–7718. [PubMed: 7644482]
4. Wang J, Lou P, Henkin J. Selective inhibition of endothelial cell proliferation by fumagillin is not due to differential expression of methionine aminopeptidases. J. Cell. Biochem. 2000; 77(3):465–473. [PubMed: 10760954]
5. Lowther WT, Mcmillen DA, Orville AM, Matthews BW. The anti-angiogenic agent fumagillin covalently modifies a conserved active-site histidine in the *Escherichia coli* methionine aminopeptidase. Proc. Natl Acad. Sci. USA. 1998; 95(21):12153–12157. [PubMed: 9770455]
6. Turk BE, Griffith EC, Wolf S, Biemann K, Chang YH, Liu JO. Selective inhibition of amino-terminal methionine processing by TNP-470 and ovalicin in endothelial cells. Chem. Biol. 1999; 6(11):823–833. [PubMed: 10574784]
7. Griffith EC, Su Z, Niwayama S, Ramsay CA, Chang YH, Liu JO. Molecular recognition of angiogenesis inhibitors fumagillin and ovalicin by methionine aminopeptidase 2. Proc. Natl Acad. Sci. USA. 1998; 95(26):15183–15188. [PubMed: 9860943]
8. Bergers G, Javaherian K, Lo KM, Folkman J, Hanahan D. Effects of angiogenesis inhibitors on multistage carcinogenesis in mice. Science. 1999; 284(5415):808–812. [PubMed: 10221914]
9. Castronovo V, Belotti D. TNP-470 (AGM-1470): mechanisms of action and early clinical development. Eur. J. Cancer. 1996; 32A(14):2520–2527. [PubMed: 9059342]
10. Konno H, Tanaka T, Kanai T, Maruyama K, Nakamura S, Baba S. Efficacy of an angiogenesis inhibitor, TNP-470, in xenotransplanted human colorectal cancer with high metastatic potential. Cancer. 1996; 77(8 Suppl):1736–1740. [PubMed: 8608571]
11. Shusterman S, Grupp SA, Barr R, Carpentieri D, Zhao H, Maris JM. The angiogenesis inhibitor TNP-470 effectively inhibits human neuroblastoma xenograft growth, especially in the setting of subclinical disease. Clin. Cancer Res. 2001; 7(4):977–984. [PubMed: 11309349]
12. Bhargava P, Marshall JL, Rizvi N. A Phase I and pharmacokinetic study of TNP-470 administered weekly to patients with advanced cancer. Clin. Cancer Res. 1999; 5(8):1989–1995. [PubMed: 10473076]
13. Kudelka AP, Verschraegen CF, Loyer E. Complete remission of metastatic cervical cancer with the angiogenesis inhibitor TNP-470. N. Engl. J. Med. 1998; 338(14):991–992. [PubMed: 9527612]
14. Logothetis CJ, Wu KK, Finn LD. Phase I trial of the angiogenesis inhibitor TNP-470 for progressive androgen-independent prostate cancer. Clin. Cancer Res. 2001; 7(5):1198–1203. [PubMed: 11350884] ■ Results from a Phase I clinical trial with TNP-470, a semisynthetic analog of fumagillin.
15. Offodile R, Walton T, Lee M, Stiles A, Nguyen M. Regression of metastatic breast cancer in a patient treated with the anti-angiogenic drug TNP-470. Tumori. 1999; 85(1):51–53. [PubMed: 10228498]
16. Schmieder AH, Caruthers SD, Zhang H. Three-dimensional MR mapping of angiogenesis with {alpha}5{beta}1({alpha}{nu} {beta}3)-targeted theranostic nanoparticles in the MDA-MB-435 xenograft mouse model. FASEB J. 2008; 22:4179–4189. [PubMed: 18697838] ■■ This work describes the theranostic potential of the perfluorocarbon nanoparticle platform in a mouse xenograft model.
17. Wickline SA, Neubauer AM, Winter P, Caruthers S, Lanza G. Applications of nanotechnology to atherosclerosis, thrombosis, and vascular biology. Arterioscler. Thromb. Vasc. Biol. 2006; 26(3): 435–441. [PubMed: 16373609]

18. Winter P, Caruthers S, Zhang H, Williams T, Wickline S, Lanza G. Antiangiogenic synergism of integrin-targeted fumagillin nanoparticles and atorvastatin in atherosclerosis. J. Am. Coll. Cardiol. Img. 2008; 1:624–634.
19. Winter PM, Schmieder AH, Caruthers SD. Minute dosages of alpha(nu)beta3-targeted fumagillin nanoparticles impair Vx-2 tumor angiogenesis and development in rabbits. FASEB J. 2008; 22:2758–2767. [PubMed: 18362202] ■■ In one of the earlier examples, it was demonstrated that a minute dosage of fumagillin is effective in treating angiogenesis in a rabbit model.
20. Lanza GM, Yu X, Winter PM. Targeted antiproliferative drug delivery to vascular smooth muscle cells with a magnetic resonance imaging nanoparticle contrast agent: implications for rational therapy of restenosis. Circulation. 2002; 106:2842–2847. [PubMed: 12451012] ■■ This paper introduces the concept of the contact-facilitated drug delivery mechanism.
21. Partlow K, Lanza G, Wickline S. Exploiting lipid raft transport with membrane targeted nanoparticles: a strategy for cytosolic drug delivery. Biomaterials. 2008; 29:3367–3375. [PubMed: 18485474]
22. Soman N, Baldwin S, Hu G. A platform of molecularly targeted nanostructures for anticancer therapy with cytolytic peptides. J. Clin. Invest. 2009; 119:2830–2842. [PubMed: 19726870] ■■ This paper reports another example of a contact-facilitated drug delivery mechanism.
23. Winter P, Neubauer A, Caruthers S. Endothelial alpha(nu)beta(3)-integrin targeted fumagillin nanoparticles inhibit angiogenesis in atherosclerosis. Arterioscler. Thromb. Vasc. Biol. 2006; 26:2103–2109. [PubMed: 16825592]
24. Zhou HF, Chan HW, Wickline SA, Lanza GM, Pham CT. Alpha v beta 3-targeted nanotherapy suppresses inflammatory arthritis in mice. FASEB J. 2009; 23(9):2978–2985. [PubMed: 19376816]
25. Zhou HF, Hu G, Wickline SA, Lanza GM, Pham CT. Synergistic effect of antiangiogenic nanotherapy combined with methotrexate in the treatment of experimental inflammatory arthritis. Nanomedicine (Lond.). 2010; 5(7):1065–1074. [PubMed: 20874021]
26. Brahn E, Schoettler N, Lee S, Banquerigo ML. Involution of collagen-induced arthritis with an angiogenesis inhibitor, PPI-2458. J. Pharmacol. Exp. Ther. 2009; 329(2):615–624. [PubMed: 19218530]
27. Kochansky J, Nasr M. Laboratory studies on the photostability of fumagillin, the active ingredient of Fumidil B. Apidologie. 2004; 35:301–310.
28. Imhof BA, Aurrand-Lions M. Angiogenesis and inflammation face off. Nat. Med. 2006; 12(2): 171–172. [PubMed: 16462798]
29. Arico-Muendel CC, Benjamin DR, Caiazzo TM. Carbamate analogues of fumagillin as potent, targeted inhibitors of methionine aminopeptidase-2. J. Med. Chem. 2009; 52(24):8047–8056. [PubMed: 19929003]
30. Hu G, Lijowski M, Zhang H. Imaging of Vx-2 rabbit tumors with alpha(nu)beta3-integrin-targeted 111In nanoparticles. Int. J. Cancer. 2007; 120:1951–1957. [PubMed: 17278104]
31. Burke J, Dennis E. Phospholipase A2 biochemistry. Cardiovasc. Drugs Ther. 2009; 23:49–59. [PubMed: 18931897]
32. Arik D, Duvdevani R, Shapiro I, Elmann A, Finkelstein E, Hoffman A. The oral absorption of phospholipid prodrugs: *in vivo* and *in vitro* mechanistic investigation of trafficking of a lecithin-valproic acid conjugate following oral administration. J. Control. Release. 2008; 126:1–9. [PubMed: 18082281]
33. Dahan A, Duvdevani R, Dvir E, Elmann A, Hoffman A. A novel mechanism for oral controlled release of drugs by continuous degradation of a phospholipid prodrug along the intestine: *in-vivo* and *in-vitro* evaluation of an indomethacin–lecithin conjugate. J. Control. Release. 2007; 119:86–93. [PubMed: 17382425] ■■ Two earlier examples of the formation of *Sn-2* phospholipid prodrugs of indomethacin and valproic acid.
34. Davidsen J, Jørgensen K, Andresen TL, Mouritsen OG. Secreted phospholipase A2 as a new enzymatic trigger mechanism for localised liposomal drug release and absorption in diseased tissue. Biochim. Biophys. Acta. 2003; 1609(1):95–101. [PubMed: 12507763]

35. Andresen TL, Davidsen J, Begtrup M, Mouritsen OG, Jørgensen K. Enzymatic release of antitumor ether lipids by specific phospholipase A2 activation of liposome-forming prodrugs. J. Med. Chem. 2004; 47(7):1694–1703. [PubMed: 15027860]

36. Jensen SS, Andresen TL, Davidsen J. Secretory phospholipase A2 as tumor-specific trigger for targeted delivery of a novel class of liposomal prodrug anticancer etherlipids. Mol. Cancer Ther. 2004; 3(11):1451–1458. [PubMed: 15542784]

37. Andresen TL, Jensen SS, Kaasgaard T, Jørgensen K. Triggered activation and release of liposomal prodrugs and drugs in cancer tissue by secretory phospholipase A2. Curr. Drug Deliv. 2005; 2(4): 353–362. [PubMed: 16305438]

38. Peters G, Møller M, Jørgensen K, Rönnholm P, Mikkelsen M, Andresen T. Secretory phospholipase A2 hydrolysis of phospholipid analogues is dependent on water accessibility to the active site. J. Am. Chem. Soc. 2007; 129(17):5451–5461. [PubMed: 17419625]

39. Garrett ER, Eble TE. Studies on the stability of fumagillin I. Photolytic degradation in alcohol solution. J. Am. Pharm. Assoc. 1954; 43(7):385–390.

40. Zelphati O, Szoka FC. Intracellular distribution and mechanism of delivery of oligonucleotides mediated by cationic lipids. Pharm. Res. 1996; 13(9):1367–1372. [PubMed: 8893276]

Patents

101. Harris TD. M Rajopadhye: US6511648. 2003

Websites

201. NCI. Developmental Therapeutics Program. www.dtp.nci.nih.gov

202. Robinson, G. Histological techniques. http://mammary.nih.gov/tools/histological/histology/index.html

Executive summary

- A novel *Sn-2* phospholipid prodrug (PD) has been synthesized by conjugating fumagillin through the *Sn-2* acyl position of an oxidized lipid, which also eliminated fumagillin light sensitivity.
- PDs were formulated in perfluorocarbon nanoparticles (NPs; ~200 nm) and studied in HUVEC cell proliferation and metabolic activity assays.
- Efficacy of $\alpha_v\beta_3$-targeted and nontargeted NPs were studied in a Matrigel™ mouse angiogenesis model.
- The fumagillin PD provided equivalent or slightly superior inhibition proliferation and viability versus the native compound when targeted to HUVECs *in vitro*.
- Integrin-targeted fumagillin-PD-NP decreased angiogenesis in a Matrigel model, while no effects were measured in the control groups as studied by MRI.
- This approach improved the photochemical and circulatory stability of fumagillin and a combination of lipid-based NPs and the PDs may facilitate the translation of NP-based antiangiogenic treatment for atherosclerosis.

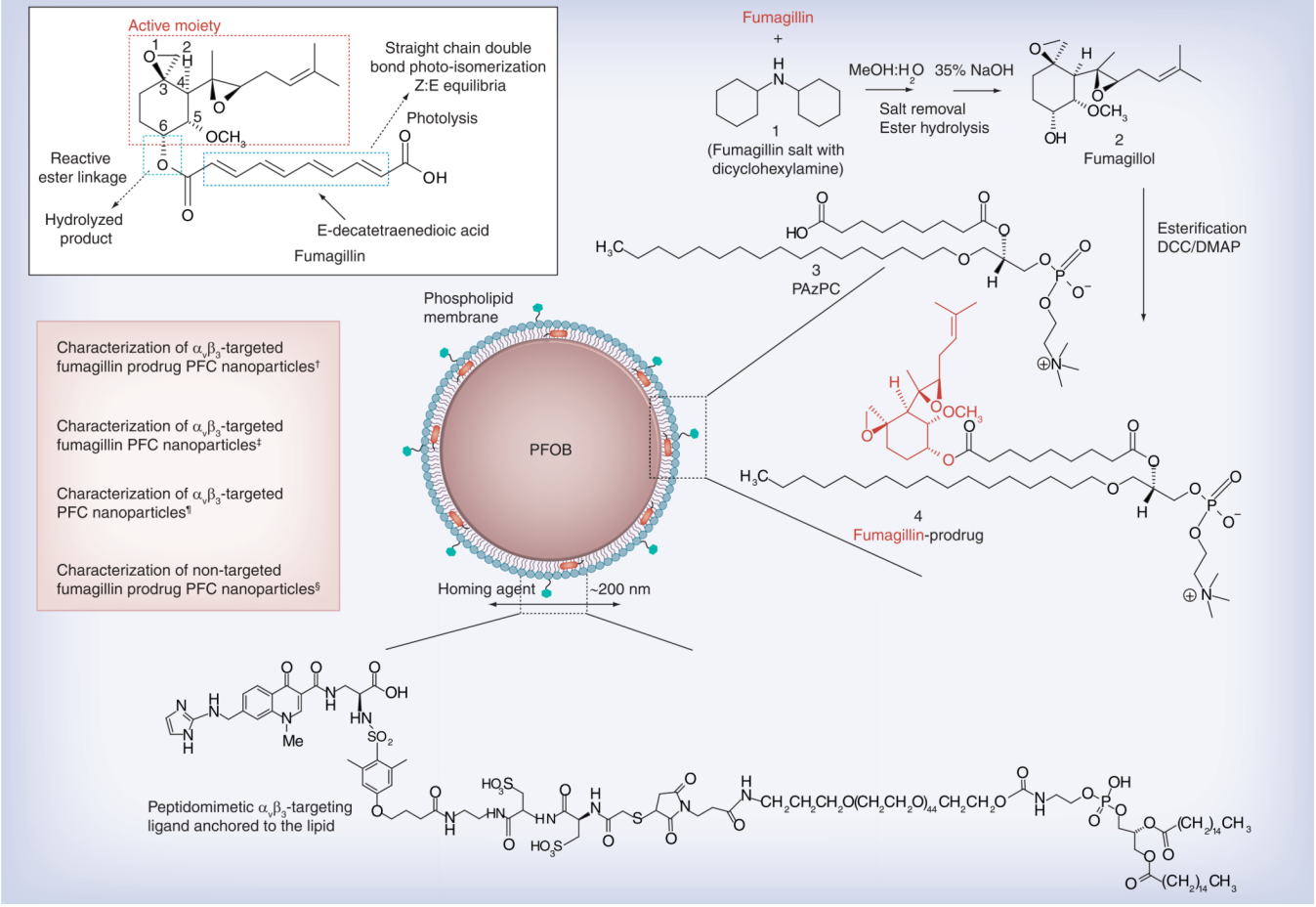

Figure 1. Structure and active sites of fumagillin with their sources of instability indicated (see figure on previous page)

Synthetic strategy for the preparation of *Sn-2* fumagillin prodrug and development of site-targeted nanoparticles: saponification of fumagillin with MeOH:water (1:1), 35% NaOH; esterification with PAzPC, DCC/DMAP; preparation of a lipid-thin film from a phospholipid mixture of 98.7 mole% lecithin phosphatidylcholine, 0.15 mole% of $\alpha_v\beta_3$-ligand-conjugated lipid and 1.12 mole% of fumagillin prodrug; self-assembly by brief sonication and microfluidization, perfluorocarbon, glycerin, pH 6.5, at 20,000 psi for 4 min.

†Hydrodynamic diameter (dynamic light scattering [DLS]): 220 nm; electrophoretic potential: −17 mV; polydispersity index: 0.19.

‡Hydrodynamic diameter (DLS): 280 nm; electrophoretic potential: −22 mV; polydispersity index: 0.25.

¶Hydrodynamic diameter (DLS): 230 nm; electrophoretic potential: −21 mV; polydispersity index: 0.06.

§Hydrodynamic diameter (DLS): 280 nm; electrophoretic potential: −10 mV; polydispersity index: 0.08.

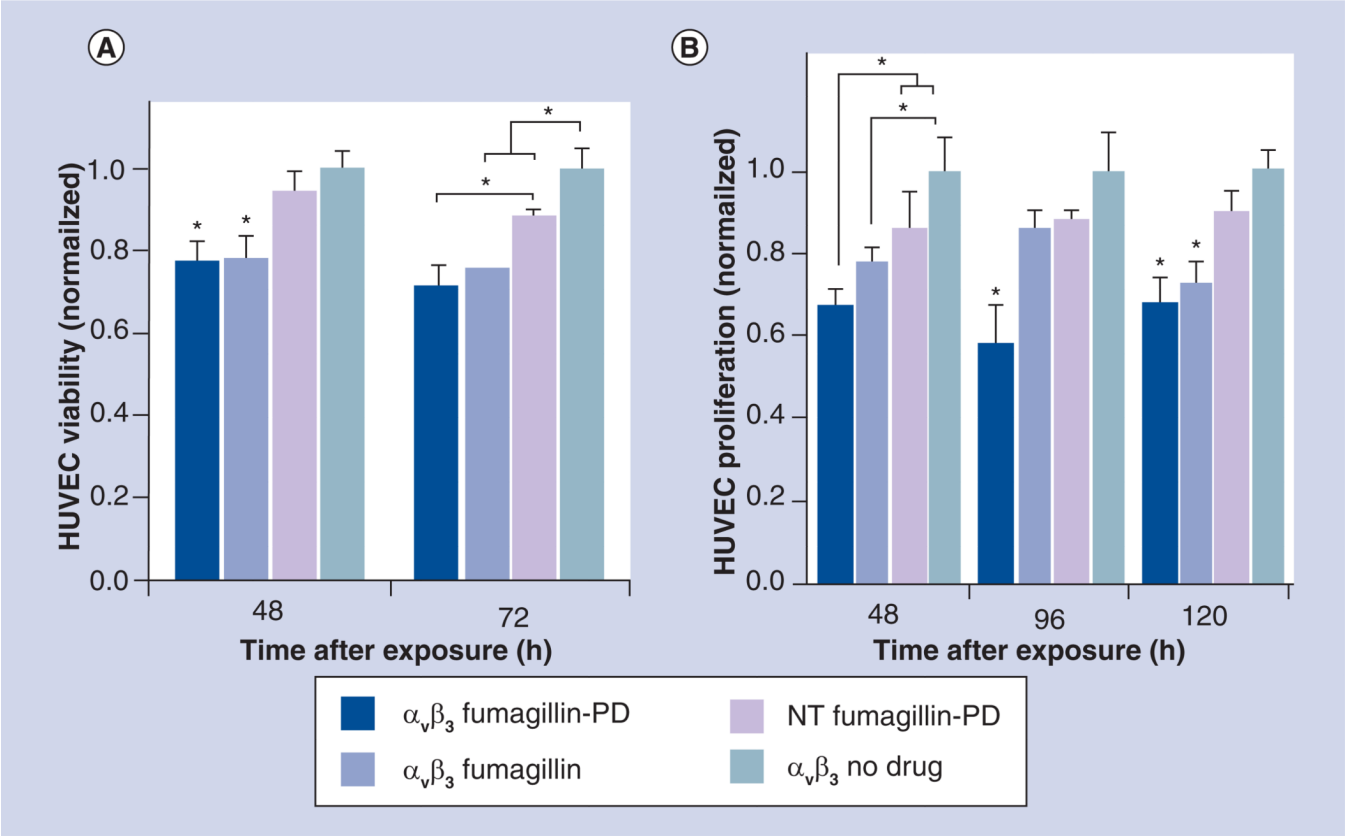

Figure 2. *In vitro* serial effect of *Sn-2* lipase-labile fumagillin prodrug-incorporated nanoparticles on HUVEC cell metabolic activity (A) and proliferation (B)

The $\alpha_v\beta_3$-targeted *Sn-2* phospholipase-labile PD nanoparticles had equivalent effectiveness *in vitro* on HUVEC **(A)** cell metabolic activity and **(B)** proliferation, compared with the $\alpha_v\beta_3$-targeted native fumagillin nanoparticles used in several previous studies [1–6]. Collectively, these data affirm the *in vitro* sensitivity of proliferating endothelial cells to the effects of $\alpha_v\beta_3$-targeted fumagillin nanoparticles, included in the native or PD form.

*$p < 0.05$ (indicates significant difference).

HUVEC: Human umbilical vein endothelial cell; NT: Nontargeted; PD: Prodrug.

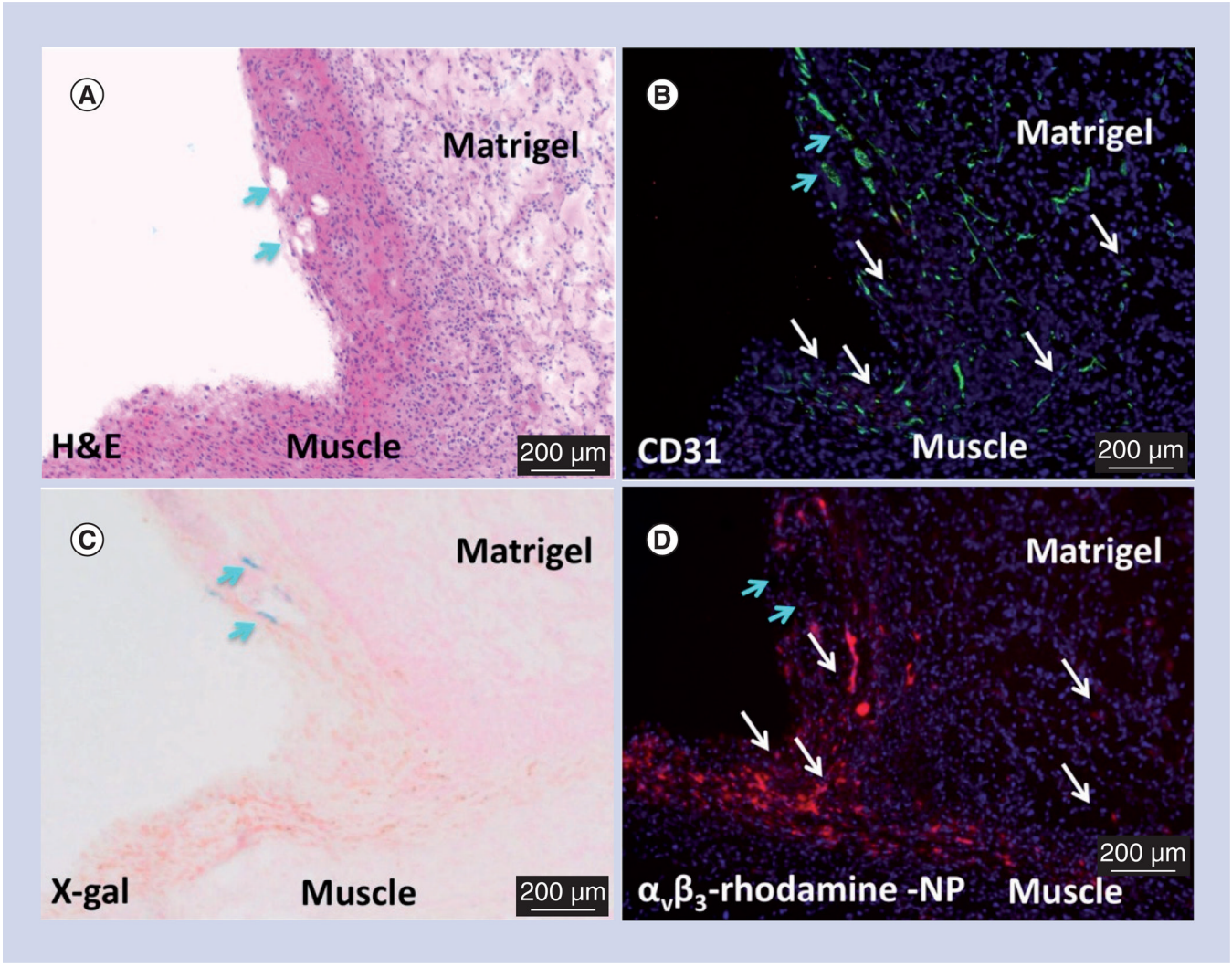

Figure 3. Microscopic examination of FGF Matrigel™ subcutaneous explant (serial sections) from FVB/N-TgN(TIE-2-LacZ)182-Sato mice following injection (intravenous) of $\alpha_v\beta_3$-targeted rhodamine-labeled perfluorocarbon nanoparticles

(A) H&E staining to illustrate the anatomic location of the implant relative to the muscle, revealing a region with prominent mature vessels (arrows). Note proliferation of inflammatory cells along the muscle and implant interface. **(B)** PECAM (CD31) staining of endothelium revealing prominent vasculature along the Matrigel periphery and the development of microvessels within the implant. **(C)** LacZ signal for β-galactosidase under Tie-2 promoter control. Lac-Z staining (arrows) is appreciated in a region of more mature vessels along the implant periphery but the signal was not observed in most of the inflammatory regions along the muscle–implant interface or within the implant. **(D)** Binding of the $\alpha_v\beta_3$-targeted rhodamine-labeled perfluorocarbon nanoparticles densely within the inflammed tissue along the muscle and implant interface and diffusely within the Matrigel implant. Regions of $\alpha_v\beta_3$-targeted rhodamine-labeled perfluorocarbon nanoparticle binding is generally correlated with areas of PECAM staining (white arrows) except for an area of rhodamine signal dropout (blue arrows) in **(D)**, which spatially paralleled prominent PECAM and LacZ staining in **(B)** and **(C)**, respectively. These images corroborate the specific binding of $\alpha_v\beta_3$-targeted nanoparticles to nascent angiogenic vessels (Tie-2^-, $PECAM^+$) and not to maturing microvessels (Tie-2^+, $PECAM^+$).

H&E: Hematoxylin and eosin; NP: Nanoparticle.

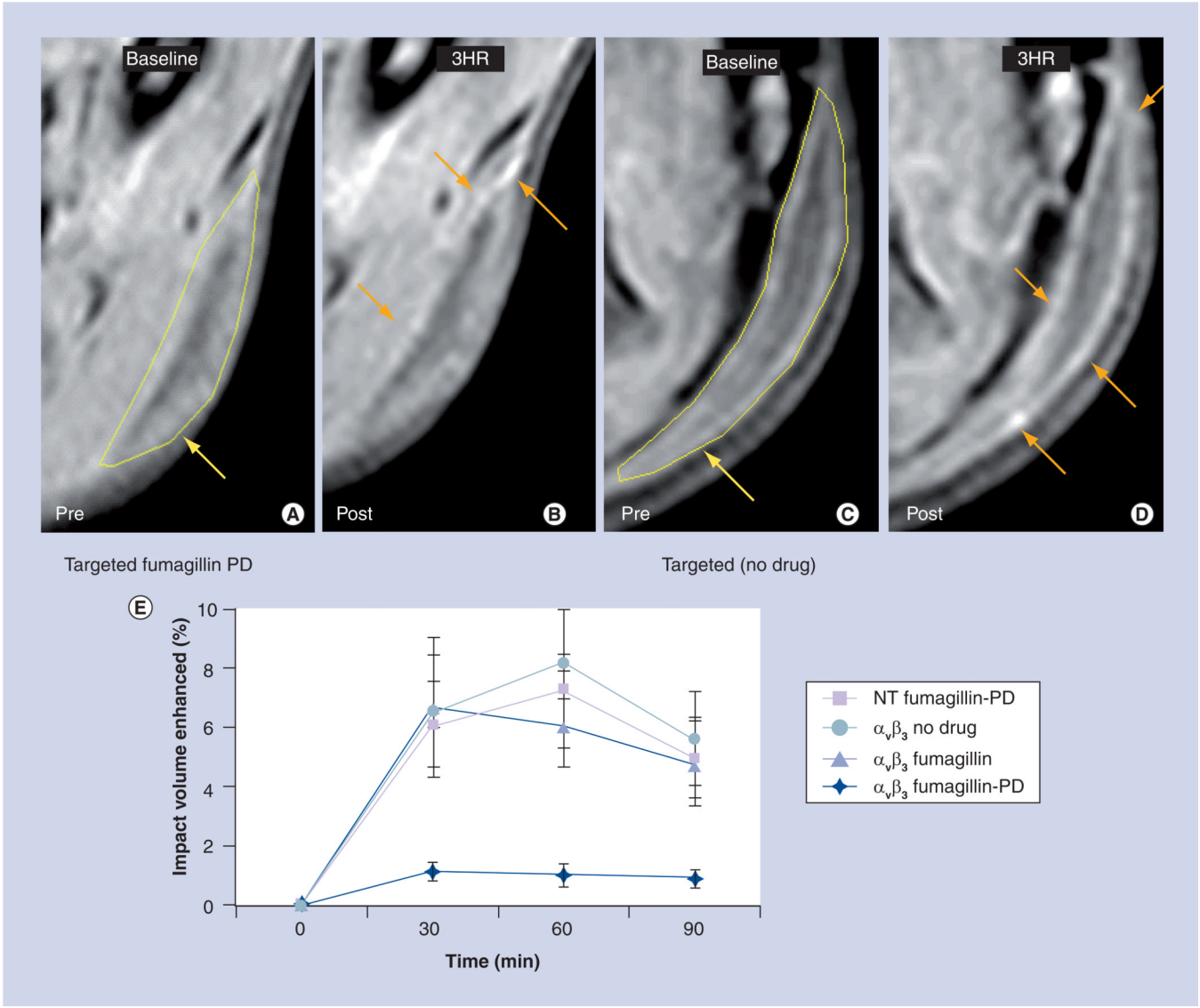

Figure 4. *In vivo* MRI study of pre- and post-treatment with targeted fumagillin prodrug nanoparticles

In vivo MR signal enhancement post-treatment with **(A & B)** targeted fumagillin nanoparticles and **(C & D)** control (no drug). In the pre-treatment images, areas of Matrigel™ implantation have been marked with yellow arrows. In the post-treatment images, signal enhancement has been denoted with orange arrows. **(E)** Reduced Matrigel implant enhancement in rats treated with $\alpha_v\beta_3$-integrin-targeted nanoparticles with fumagillin-PD versus $\alpha_v\beta_3$-integrin-targeted nanoparticles with fumagillin, $\alpha_v\beta_3$-integrin-targeted nanoparticles without drug and nontargeted nanoparticles with fumagillin-PD. NT: Nontargeted; PD: Prodrug.

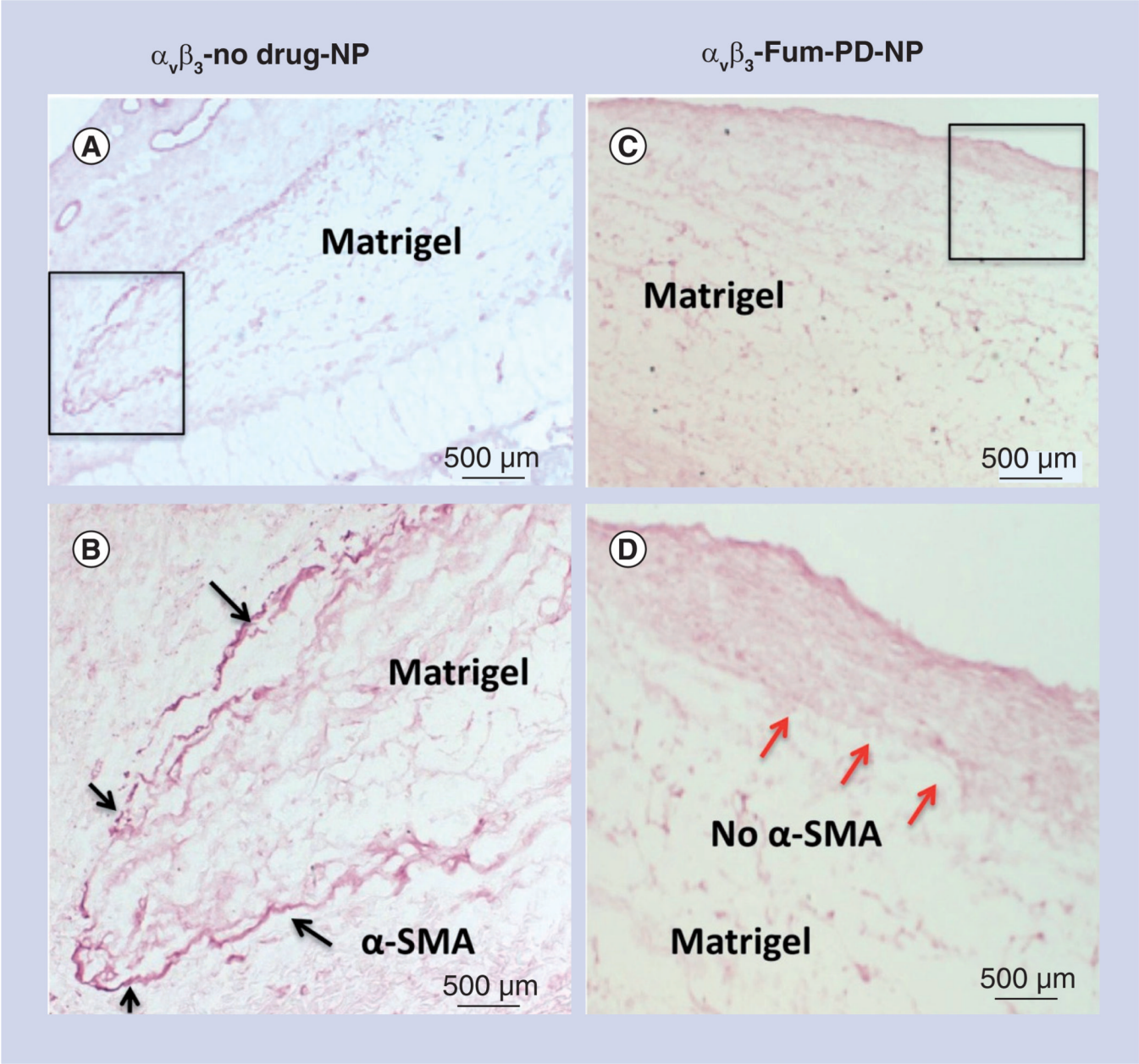

Figure 5. Microscopic examination of FGF Matrigel™ subcutaneous explant in mice following serial injection (intravenous) of $\alpha_v\beta_3$-targeted no-drug perfluorocarbon nanoparticles ($\alpha_v\beta_3$-no drug-NP) or $\alpha_v\beta_3$-targeted fumagillin prodrug perfluorocarbon nanoparticles ($\alpha_v\beta_3$-Fum-PD-NP)

(A) Low power image of Matrigel™ explant from control animal that was immunostained to identify maturing vessels with α-SMA. Positive staining was appreciated peripherally around the majority of the plug (black box). **(B)** Enlarged view of boxed region in **(A)**, showing the peripheral α-SMA biomarker. **(C)** Low power image of Matrigel explant from fumagillin PD-treated animal that was immunostained to identify maturing vessels with α-SMA. Virtually no positive staining was appreciated along the implant periphery, suggesting that the repeated pruning of angiogenic vessels with fumagillin PD impaired the development and progression of mature vessels in contrast with the control. **(D)** Enlarged

view of boxed region in **(C)**, illustrating the lack of peripheral α-SMA biomarker (red arrows).
α-SMA: α-smooth muscle actin; NP: Nanoparticle; PD: Prodrug.